Asynchronous haptic simulation of contacting deformable objects with variable stiffness

Igor Peterlik, Christian Duriez, Stéphane Cotin

Asynchronous Haptic Simulation of Contacting Deformable Objects with Variable Stiffness

Igor Peterlík, Christian Duriez, Stéphane Cotin

Abstract— This paper presents a new asynchronous approach for haptic rendering of deformable objects. When stiff non-linear deformations take place, they introduce important and rapid variations of the force sent to the user. This problem is similar to the stiff virtual wall for which a high refresh rate is required to obtain a stable haptic feedback. However, when dealing with several interacting deformable objects, it is usually impossible to simulate all objects at high rates. To address this problem we propose a quasi-static framework that allows for stable interactions of asynchronously computed deformable objects. In the proposed approach, a deformable object can be computed at high refresh rates, while the remaining deformable virtual objects remain computed at low refresh rates. Moreover, contacts and other constraints between the different objects of the virtual environment are accurately solved using a shared Linear Complementarity Problem (LCP). Finally, we demonstrate our method on two test cases: a snap-in example involving non-linear deformations and a virtual thread interacting with a deformable object.

I. INTRODUCTION

Haptic rendering on deformable objects has numerous applications. For instance, in medicine, it could be integrated to a training system for high-fidelity interactions with virtual soft-tissues. However, several scientific challenges are still preventing the development of such simulations, such as precise modeling of the deformations, collision detection and accurate contact response between deformable structures, which are generally too computationally demanding to achieve real-time simulations. Moreover, rendering algorithms allowing for stable and realistic haptic feedback are usually not compatible with such simulations, as they ask for much faster refresh rates than what is achievable by the other components of the simulation. One way to overcome this difficulty is to desynchronize the computation of the haptic rendering from the computation of the remaining components (computed at slower rates) using various *local models*. However, there are some limitations with these methods, especially when one of the deformable objects is light and stiff.

Let us take the example, illustrated by Fig 1, of a virtual thread attached at one end to a fixed support and controlled at the other end by the haptic device. A characteristic of a thread or very thin cable is that it has a very low bending energy but high stretching energy. As a consequence, a nearly null haptic force is generated during bending. But when the

user pulls, on the thread a stiff force appears very suddenly when the thread is straightened out. The haptic rendering of this example can be compared to the well known problem of virtual walls: to obtain a stiff rendering, one needs to increase the frequency of its simulation in the haptic control loop. In other words, in our example, the simulation rate of the entire thread needs to be very high (e.g. 1kHz, about the same frequency as for virtual walls) to be able to reproduce this rapid change in stiffness during the manipulation of the virtual thread. Assuming this is possible for the thread model, the rest of the simulation (the other deformable models, the collision detection and response) will most likely need to be updated at slower rates (i.e. ≈ 50Hz) due to their complexity. This example is not unique in haptic-based simulation of deformable objects where there is a need for adapting the refresh rate of each object depending on the characteristic of its deformations. That is why we introduce a technique that maintains a coherency between interacting deformable models that are simulated in real-time but at various frequencies.

In [1], we present a constraint-based rendering technique using compliance[1], within a multithreaded environment. The simulation of the deformations, the collision detection and response are computed in a low rate loop. In the haptic loop. a fast update of the constraints is performed at high rates based on the measured position of the device.

In this paper, the idea of constraint-based rendering using compliance of the objects is still preserved. But the main difference is that the deformable objects are simulated at different frequencies. We demonstrate our method with the interactions between two different deformable models: a *curved deformable object*, guided by the haptic device motion, which is simulated at high rates and a *volumetric obstacle* is computed in a low-rate loop. It results in a true multi-rate asynchronous simulation of deformable objects: each object can be updated at an independent refresh rate. The main contribution of the paper is the contact process that allows for accurate collision response regardless the respective update rate of the objects.

II. PREVIOUS WORK

The approach presented in this paper focuses on realistic haptic rendering involving deformable objects in contact simulated on different frequencies. In this section we provide an overview of methods proposed in the area of haptic rendering, starting with approaches geared toward stable

---

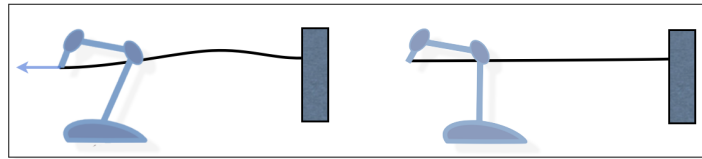[1]The compliance is the inverse of the stiffness.

Fig. 1. Cable-based virtual wall. Left: the cable is loosely bended; almost no response force is perceived. Right: the cable is stretched, the force is sharply increased as the transition between bending and stretching occurs (analogy to virtual wall).

realistic haptic rendering of contacts between rigid bodies, and followed by a brief survey of techniques used for the haptic rendering of deformable objects.

Haptic interaction in virtual environment that involves contacts with various objects has been well studied. The coupling between the device and the virtual scene is one of the key aspects. In [2], a concept of *virtual coupling* has been proposed. Originally designed to improve the haptic rendering of virtual walls, it can be regarded as an artificial mechanical coupling connecting the haptic device and the virtual object. A *god-object* approach is introduced in [3] to increase the perception of stiffness. In this case the haptic interface is represented by a 3DoF virtual model (the god-object) which conforms to the virtual environment. The method is extended by the technique of *virtual proxy* in [4]. Another extension of the god-object towards 6-DoF rendering is represented by a *constrained-based* method introduced in [5]. It is based on a minimization of the kinetic distance between the actual position of the haptic device and virtual proxy. The method results in realistic contact modelling by enforcing the non-penetration constraint between the objects.

In pioneering works on realistic haptic rendering of deformable bodies, simplified boundary conditions are usually employed instead of contact modeling. E.g. in [6], [7], *displacement-driven* interaction is considered, so the positions are applied as bilateral constraints (equality conditions) and solved by a method of Lagrange multipliers. In [8], a unified approach to the interaction with elastostatic contact simulation is presented. In this case, the contact resolution is based on *capacitance matrix* which relates the imposed displacements and response forces. The method is used for single-point as well as grasping interaction, where haptic rates are achieved using precomputed Green functions. In [9], the contact problem is solved using a penalty-based method allowing for multiple contacts and self-collisions. Both tool and obstacle are deformable, being simulated by finite elements methods optimized by model reduction [10].

In order to guarantee the non-interpenetration, constrained-based methods are used for contact handling. Higher cost of the methods is addressed by multi-rate approach. Although efficient multi-rate methods have been proposed to model complex contacts in physically correct and accurate way (e.g. [11]), real-time haptic interaction based on these models remains challenging due to the stability issues [12].

In [13], a multilayer finite element is used to decouple finer and coaser regions for linear models. It is shown that each layer can be computed on different frequency. To increase the haptic fidelity in [14], full non-linear model is simulated at low frequency, whereas linearized approximation is updated on high rate. In [15], a method based on adaptive multi-rate integration is proposed. A hierarchy of non-nested tetrahedral meshes is used: the high-resolution meshed are employed locally in the regions where high stress occurs. In [16], a multi-rate method allowing for rendering of rigid tool in contact with compliant environments is presented, considering only the equality constraints without friction. The constraint-based collision response is calculated in the low-rate visual loop, while linear contact model is solved in each iteration of the haptic loop, relying on intermediate representations (inverse of the contact Jacobian in this case) provided by the low-rate collision response. In [17], haptic rendering for non-linear deformable model is proposed for medical application. The method uses an approximation of the compliance matrix and a *Linear Complementarity Problem* (LCP) is shared between the simulation and the haptic loop. In [18] both the tool and the obstacle are considered as deformable objects that can undergo large deformations. However a part of the deformable tool (a *handle*) needs to be rigidified to be connected to the haptic device by viscoelastic link [19]. Contact simulation is based on a simplification of the inverse matrix (similar to the compliance matrix) as only diagonal blocks are considered. Thus, indirect contacts cannot be rendered and the computation of the direct contact force is not accurate, especially for light and stiff objects.

In [20], a multi-rate approach is proposed for friction contact modelling with deformable body. A linearization and model reduction is used to obtain the inter-sample behaviour between two steps of the slower simulation loop. A precise multi-rate interaction with textile models is studied in [21]. Intermediate level is introduced to determine the behaviour of the tissue part which is in direct interaction with the user.

Despite the progress in computer performance, the realistic simulation of complex environments including deformable objects with different stiffness within the haptic loop is still out of reach. The methods proposed so far allow for computing the haptic feedback using the non-linear deformable models. Nevertheless, the results are usually demonstrated only for soft deformable objects. We believe that realistic stable rendering of stiff models is also necessary for convincing haptic feedback, however, it puts higher requirements on stability of the interaction. Therefore, we propose a novel multi-rate technique allowing for stable haptic rendering of complex interactions among rigid and deformable objects being simulated at different rates.

III. Quasi-static and Asynchronous Deformable Models in Contact

The mathematical formulation together with description of the deformable models are introduced in this section. It is assumed that there is at least one deformable object which is attached to the haptic device and it can be simulated at high frequency (such as $1000\,\mathrm{Hz}$). The other objects with more complex behavior are modeled at lower frequencies (e.g. $50\,\mathrm{Hz}$).

In order to simplify the explanation, following scenario is supposed: the haptic device is connected to deformable curve-like beam object (such as clip or suture thread) which is simulated at high-frequencies. This object interacts with deformable volumetric object which is simulated at low rates. The model used for both objects allows for large deformations.

It should be emphasized that the method is not limited to this scenario; for instance volumetric linear deformable models, computed at high rates can be employed instead of the beam model.

Throughout the paper, following notation is used: $\mathbf{M}_v$ and $\mathbf{v}_c$ represent a matrix associated to the volumetric object and a vector associated to the curve model, respectively. Moreover, the left superscript L in $^L\mathbf{M}$ indicates that the matrix is computed at low rates (superscript H is used for high rates). Finally, left subscript is used if the structure is buffered between the threads: matrix $^H_L\mathbf{M}$ was computed at high rates (superscript H) and it is accessed from the low-rate thread (subscript L) via buffer.

A. Volumetric deformation at low rate

The non-linear deformation of the volumetric object is computed using a corotational finite element approach. In this approach, a rotation is estimated during the deformation, for each element of the mesh. At the level of the element, the deformation remains linear but the computed rotations add a non-linear part to the global model (after assembling each element). This approach allows for handling large deformations with small strain. During the simulation, the following linearization of the global model is computed at each step:

$$\mathbf{f}_v(\mathbf{x_t}) \approx \mathbf{f}_v(\mathbf{x_{t-1}}) + \mathbf{K}_v(\mathbf{x_{t-1}})d\mathbf{x} \tag{1}$$

where $\mathbf{f}_v$ provides the volumetric internal stiffness forces at a given position $\mathbf{x}$ of the nodes, $\mathbf{K}_v(\mathbf{x})$ is the tangent stiffness matrix that depends on the actual position of the nodes and $d\mathbf{x}$ is the difference between positions in two time steps $d\mathbf{x} = \mathbf{x_t} - \mathbf{x_{t-1}}$.

A damping matrix $\mathbf{B}_v$ is introduced into the formulation [2]. We obtain the following differential equation:

$$\mathbf{B}_v\dot{\mathbf{x}} + \mathbf{f}_v(\mathbf{x}) + \mathbf{p} + \mathbf{J}_v^T\boldsymbol{\lambda} = 0 \tag{2}$$

where $\mathbf{p}$ represents the external forces (e.g. gravity) and $\mathbf{J}_v^T\boldsymbol{\lambda}$ gathers the contributions of the contact forces applied to the

[2]Damping matrix $\mathbf{B}_v$ is similar to the mass matrix obtained by lumping technique.

object. The backward Euler integration scheme of the 1st order is used with a time step h_L set according to the low frequency being used. It leads to the following equation:

$$\underbrace{\left[-\frac{1}{h_L}\mathbf{B}_v - \mathbf{K}_v(\mathbf{x_{t-1}})\right]}_{\mathbf{A}_v} d\mathbf{x} = \mathbf{p} + \mathbf{f}_v(\mathbf{x_{t-1}}) + \mathbf{J}_v^T\boldsymbol{\lambda}. \tag{3}$$

It should be noticed that the matrix on the left side of the equation is highly sparse, so an efficient direct solver can be applied to solve the system. For a reasonable number of points (≈ 50 ?) and tetrahedral elements (≈ 300 ?) the computation can be done at $50Hz$, so $h_{LR} = 0.02$.

B. Curve deformable model

The model used to simulate the deformation of a curve-like object at high rates is also based on a FEM approach, which has similarities with the volumetric model. The curve is modeled using serially-linked beam elements, each beam being defined by two 6 DoF nodes, one of the nodes defining a local frame. In this frame the deformation remains linear but after rotating and assembling the beams, the model can handle the non-linearities caused by large rotations. The resulting equations are similar to those presented for the volumetric model. We also use the backward Euler scheme for time integration, except that the time step h_H is much smaller, corresponding to high rates (typically $1000\,\mathrm{Hz}$). Moreover, the model is coupled to the 6 DoF position of the haptic device using a damped spring. The integration method results in following equation determining the behaviour of the curved object:

$$\underbrace{\left[-\frac{1}{h_H}{}^H\mathbf{B}_c - {}^H\mathbf{K}_c(\mathbf{x_{t-1}})\right]}_{{}^H\mathbf{A}_c} d\mathbf{x} = \mathbf{p} + {}^H\mathbf{f}_c(\mathbf{x_{t-1}}) + {}^L_H\mathbf{J}_c^T\boldsymbol{\lambda}. \tag{4}$$

where $\mathbf{B}_c$ and $\mathbf{K}_c$ are tri-diagonal band matrices. In this case, optimized tri-diagonal direct solver can be used to perform an efficient solution of the system composed of about 30 elements, being suitable for the short time step h_H, typically $1\,\mathrm{ms}$.

To avoid synchronization problems during the interactions between low-rate and high-rate object, a *proxy* of the high-rate body is introduced. It can be regarded as an interface of the curve object that provides information needed for contact collision and response computed at low rates. Finally, it should be noted that matrix $^L_H\mathbf{J}_c^T$ is computed at low-rates, but it is available in the high-rate loop via buffer.

C. Contact process

The contact process begins with a proximity queries algorithm that is computed at low rates. For the proxy, we use the position that was stored at the end of the previous simulation step. All detected pairs of close points are considered as being potentially in contact. The directions of the contacts are stored in the matrices $\mathbf{J}^T$ for each object involved in the interaction[3].

[3]The direction is mapped to the FE nodes using barycentric coordinates if the contact point does not coincide with any FE node.

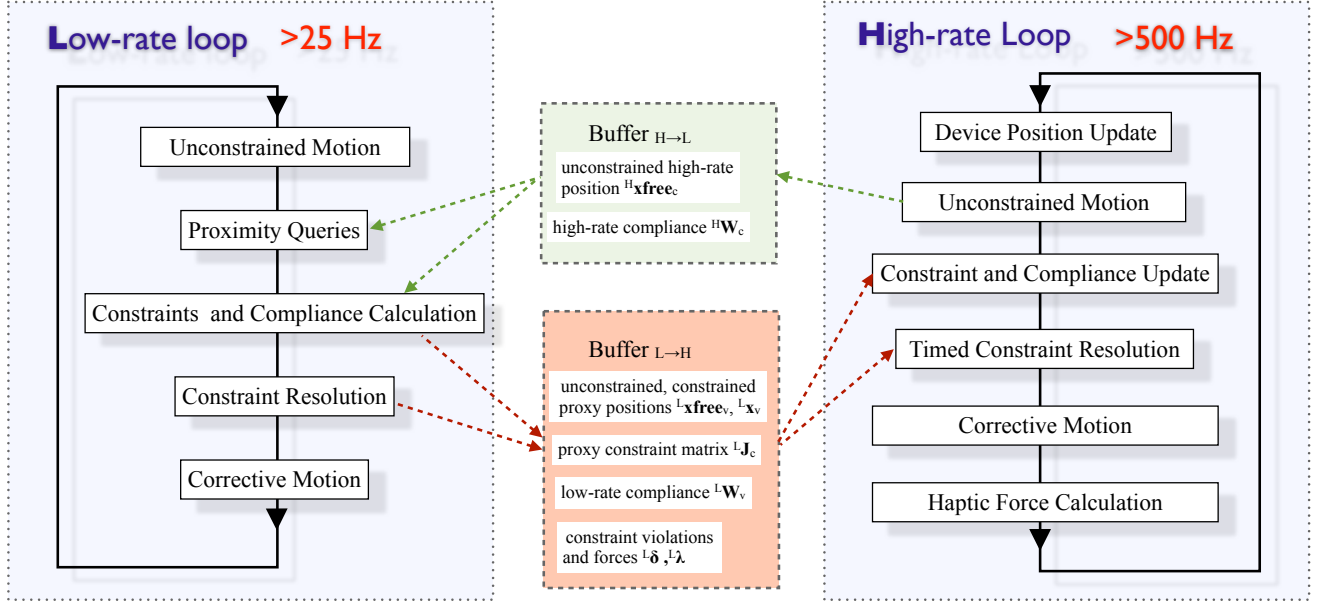Fig. 2. Schematic visualization of the computational model.

For the contact response, we apply the Signorini's law $0 \leq \boldsymbol{\delta} \perp \boldsymbol{\lambda} \geq 0$, where $\boldsymbol{\delta}$ is the vector that gathers the distances at each pair of contacting points. The thickness of the curve model is subtracted from the computation of $\boldsymbol{\delta}$.

In order to solve the Signorini's law, we need what is called the free position of both objects. For the volumetric object, it is obtained by solving equation (3) with $\boldsymbol{\lambda} = 0$ and computing $\mathbf{x}_v^{\text{free}} = \mathbf{x_{t-1}} + d\mathbf{x}$. For the curve deformable model, the same technique is applied using Eq.(4), except that for the proxy, the position $_L^H\mathbf{x}_c^{\text{free}}$ obtained in the last iteration of the high-rate loop is used. This means, however, that $\mathbf{x}_v^{\text{free}}$ and $_L^H\mathbf{x}_c^{\text{free}}$ do not necessary correspond to the same time $\mathbf{t}$.

Given the free positions for both objects, the contact violations $\boldsymbol{\delta}^{\text{free}}$ are computed for each pair of close points. The contact process executed at low rates builds the following LCP:

$$\begin{cases} \boldsymbol{\delta} = \left[\mathbf{J}_v\mathbf{A}_v^{-1}\mathbf{J}_v^T + \mathbf{J}_c\{_L^H\mathbf{A}_c^{-1}\}\mathbf{J}_c^T\right]\boldsymbol{\lambda} + \boldsymbol{\delta}^{\text{free}} \\ \qquad\qquad 0 \leq \boldsymbol{\delta} \perp \boldsymbol{\lambda} \geq 0. \end{cases} \quad (5)$$

The compliance[4] of the curve model $\mathbf{A}_c^{-1}$ is computed at high rates but buffered to be accessible from the low-rate thread. The LCP is first solved by Gauss-Seidel-like solver at low rates, resulting in solution vector $^L\boldsymbol{\lambda}$. Then, the positions of both volumetric model $\mathbf{x}_v$ and curve object proxy $^L\mathbf{x}_c$ are updated using $\mathbf{x} = \mathbf{x}^{\text{free}} + \mathbf{A}^{-1}\mathbf{J}^T\{^L\boldsymbol{\lambda}\}$. Note that the position computed for the proxy is now synchronized with the position of the volumetric object. It is then stored to be used in the proximity queries in the next time step.

Moreover, the LCP is also shared with the high-rate loop and recomputed according to the curve object deformations. In that case, the compliance of the volumetric object

computed and buffered at low rates is used, i.e. $_H^L\mathbf{W}_v = \{^L\mathbf{J}_v\}\{^L\mathbf{A}_v^{-1}\}\{^L\mathbf{J}_v^T\}$. However, for the curve object, the compliance is updated according to the actual configuration, i.e. $^H\mathbf{W}_c = \{_H^L\mathbf{J}_c\}\{^H\mathbf{A}_c^{-1}\}\{_H^L\mathbf{J}_c^T\}$. Thereby, the deformations obtained at high rates also follow the contact law with a new value of the constraints $^H\boldsymbol{\lambda}$. It should be noted that the directions of the contacts are computed in low-rate thread and only contact distances are updated at high-rates. This can be regarded as a limitation of the method w.r.t. the fidelity of contact modeling.

IV. COMPUTATIONAL MODEL

In this section, our asynchronous multi-rate approach is described from the algorithmic point of view. To simplify the explanation, the same bodies (volumetric and curve-like) are involved in the interaction.

A. Multi-rate interaction scheme

To build this multi-rate scheme, two different loops are launched in separate threads: a simulation loop, at low rates and the haptic loop, at high rates (see figure 2). As stated before, we introduce a proxy of the curve model in the simulation loop that provides a representation of the curve model that is computed in the haptic loop.

The computations performed in one step of the simulation loop are executed as follows:

S1 The free position vectors of both simulated bodies are obtained: for the volumetric object, the free motion is computed resulting in $^L\mathbf{x}_v^{\text{free}}$ and factorization of the system matrix $^L\mathbf{A}_v$. For the curved object, the actual buffered free position vector $_L^H\mathbf{x}_c^{\text{free}}$ and inversed matrix $_L^H\mathbf{A}_c^{-1}$ are provided by the buffer $_L^H\mathcal{B}$ stored in the last iteration of the haptic loop.
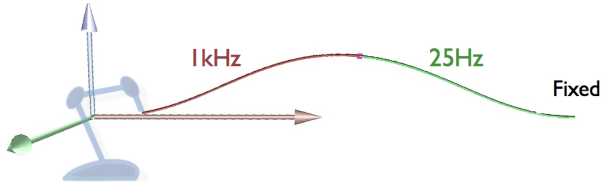
---

[4]$\mathbf{A}_c$ is homogeneous to the stiffness

Fig. 3. Validation of action-reaction principle. The deformations of low-frequency object (green) and high-frequency object (red) are the same.

Fig. 4. Illustration of the snap-in example. The clip is simulated at 1000 Hz whereas the cylinder is simulated at 25 Hz.

S2 The simulation thread executes the proximity queries between the volumetric and curved object, using the proxy position $^L\mathbf{x}_c$ and $^L\mathbf{x}_v$. The constraint violations $^L\boldsymbol{\delta}^{\text{free}}$ are computed together with constraint matrices $^L\mathbf{J}_c$ and $^L\mathbf{J}_v$ for each object.

S3 For both volumetric and curved object, compliance matrices projected onto the constraint space are computed respectively: $^L\mathbf{W}_c = \{^L\mathbf{J}_c\}\{^H_L\mathbf{A}_c^{-1}\}\{^L\mathbf{J}_c^\top\}$, $^L\mathbf{W}_v = ^L\mathbf{J}_v\{^L\mathbf{A}_v^{-1}\}^L\mathbf{J}_v^\top$.

S4 The full constraint resolution is performed using the operator $^L\mathbf{W} = {}^L\mathbf{W}_c + {}^L\mathbf{W}_v$ and vector $^L\boldsymbol{\delta}^{\text{free}}$ of the constraint violations, resulting in vector $^L\boldsymbol{\lambda}$ of the Lagrange multipliers representing the contact forces.

S5 The corrective motion is performed using $^L\boldsymbol{\lambda}$ resulting in interpenetration between the free positions of the volumetric object ($^L\mathbf{x}_v$) and the proxy of curved object ($^L\mathbf{x}_c = {}^H_L\mathbf{x}_c^{\text{free}} + \{^H_L\mathbf{A}_c^{-1}\}\{^L\mathbf{J}_c^\top\}^L\boldsymbol{\lambda}$)

S6 The unconstrained position $^H\mathbf{x}_c^{\text{free}}$ and the constraint matrix $^L\mathbf{J}_c$ of the curved object are stored into the buffer $^L_H\mathcal{B}$. The projected compliance of the volumetric objects $^L\mathbf{W}_v$ together with constraint violations $^L\boldsymbol{\delta}^{\text{free}}$ and forces $^L\boldsymbol{\lambda}$ are buffered as well, as they will be updated in the haptic loop.

In parallel, the haptic loop performs computations concerning the high-rate object, using the actual position of the haptic device and data structures stored in the buffer $^L_H\mathcal{B}$ in the last iteration of the simulation loop.

H1 The position of the coupling spring is updated according to the actual position of the haptic device.

H2 The free motion of the curved model is computed resulting in a vector of free position $^H\mathbf{x}_c^{\text{free}}$ that is stored to buffer $^L_H\mathcal{B}$ together with the inverse $^H\mathbf{A}_c^{-1}$.

H3 The updated constraint violation vector $^H\boldsymbol{\delta}^{\text{free}}$ is computed using the actual position of the curved object $^H\boldsymbol{\delta}^{\text{free}} = {}^L_H\boldsymbol{\delta}^{\text{free}} + {}^L_H\mathbf{J}_c(^H\mathbf{x}_c^{\text{free}} - {}^H_L\mathbf{x}_c^{\text{free}})$.

H4 The updated projected compliance of the curved object $^H\mathbf{W}_c$ is computed using the new inverse of the stiffness matrix obtained in the step H2: $^H\mathbf{W}_c = {}^L_H\mathbf{J}_c[^H\mathbf{A}_c^{-1}]^L_H\mathbf{J}_c^\top$.

H5 The updated vector of Lagrange multipliers $^H\boldsymbol{\lambda}$ is computed by a time-limited contact resolution, using updated data $^H\boldsymbol{\delta}^{\text{free}}$ and operator $^H\mathbf{W} = {}^L_H\mathbf{W}_v + {}^H\mathbf{W}_c$. The vector $^L_H\boldsymbol{\lambda}$ is used as the initial estimation computed to improve the convergence of the times constraint resolution.

H6 The haptic force feedback $\mathbf{f}$ is computed: first, the corrective motion of the high-rate object is performed
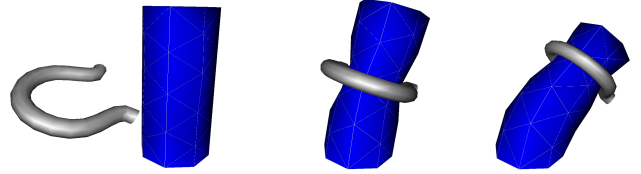
to obtain $^H\mathbf{x}_c$. Then, the actual force is computed as the elastic force of the coupling spring. An alternative calculation of the force feedback is proposed below.

B. Haptic force feedback

Several remarks concerning the computations in the haptic thread are presented below. Since the quasi-static deformations of the high-rate object are performed directly in the haptic loop, deformation model must be fast enough to keep the haptic rate. However, complexity of the computations of the haptic loop also depends on the number of contacts. There are two ways to minimize the influence of this parameter. First, the compliance update performed in H4 is computed efficiently exploiting the sparsity of matrices. Second, the *timed version* of the constraint resolution is executed in the step H5: the Gauss-Seidel iterative process is stopped after given amount of time regardless of convergence. It is important to recall, that the timed Gauss-Seidel method uses $^L\boldsymbol{\lambda}$ as the initial estimation. Therefore, if the motion of the haptic device is quite slow w.r.t. the refresh rate of the simulation loop, the solution provided between two steps does not vary too fast. Hence, it can be assumed that the convergence of the timed Gauss-Seidel method can be achieved in given amount of time.

V. RESULTS

In the following, experiments are presented in order to demonstrate the multi-rate approach proposed in this paper.

First, the validation of *action-reaction* principle has been performed using two beam models having the identical physical properties, each being calculated at different frequency. The low-rate curve-like object was fixed in the space, whereas the high-rate one was attached to the low-rate body on one end and to the haptic device on the other. Although each model was calculated at different frequency, the deformations of both objects was identical for arbitrary position of the haptic device as shown in Fig. 3.

Second, we implemented a snap-in scene, depicted in Fig. 4. In this example, the high-rate object was represented by a stiff but deformable clamp attached to the haptic device via coupling spring. The clip was modeled with 20 corotational beam elements and nodes with positional and rotational degrees of freedom were used in the model. As the obstacle, a deformable cylinder composed of 103 tetrahedral elements was simulated. During the snap operation, up to 20 constraints were created.
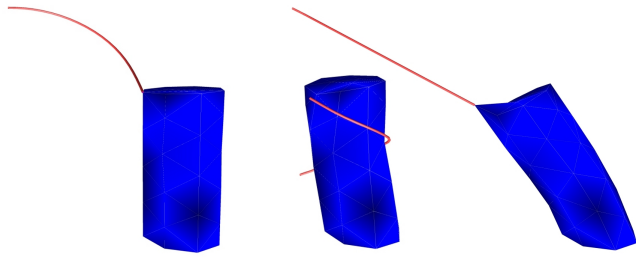
Fig. 5. Illustration of the scene composed of cylinder (simulated at a rate of 25 Hz) and the thread (simulated at 1000 Hz).

Various rigidities of both cylinder and clamp were tested with haptic feedback. This example shows that we are able to model complex contact problem between objects which are simulated at various refresh rates. Moreover, even with stiff mechanical properties for the clamp, the haptic rendering remains stable; it should be noted, however, that the properties of the damped spring used for coupling between the haptic interaction point and clamping tool were adapted accordingly.

Further, our approach was validated using a scene with thread and deformable cylinder. The thread was modeled with 10 beam elements (computed at 1000 Hz) and cylinder described in the previous example was used (simulated at 50 Hz). One end of the thread was attached to the cylinder, while the other end was manipulated by the haptic interface. Beside the bilateral constraint between the thread and cylinder, a contacts between the two objects were detected and resolved resulting in more complex interaction. Despite the complexity of the simulation, both stable and realistic haptic force feedback was delivered to the user.

The simulation was performed for the scenario where the thread was also computed at low rates (50 Hz). In this case it was observed that the simulation became rapidly unstable. This instability appeared mainly in the moment when the user rapidly pulled the thread, changing its configuration from loosely bended to stretched.

We think that the beam model displays an important change in stiffness during very short time when the deformation is changed from bending to stretching. To handle this transition correctly, the simulation must be run at high rates, as was demonstrated by our experiments. Nevertheless, with increasing stiffness of the thread, even the frequency of 1 kHz might not be sufficient and higher rates would be needed to guarantee the stability during the pulling procedure.

VI. CONCLUSION AND FUTURE WORK

In this paper, a novel approach to the accurate multi-rate haptic rendering of non-linear deformable models in contact was presented. Since the method is based on Signorini's law, the non-penetration is guaranteed. It was demonstrated that the stability of the haptic feedback is achieved even for stiff objects.

In the future, we will investigate the extension of the method towards dynamic models. We will also plan to employ the method for the simulation of suturing.

REFERENCES

[1] I. Peterlík, C. Duriez, and S. Cotin, "Constraint-based haptic rendering of multirate compliant mechanisms," to appear in IEEE.Trans. on Haptics, 2011.
[2] J. Colgate, M. Stanley, and J. Brown, "Issues in the haptic display of tool use," *Intelligent Robots and Systems, IEEE/RSJ International Conference on*, vol. 3, p. 3140, 1995.
[3] C. B. Zilles and J. K. Salisbury, "A constraint-based god-object method for haptic display," in *IROS '95: Proceedings of the International Conference on Intelligent Robots and Systems-Volume 3*. Washington, DC, USA: IEEE Computer Society, 1995, p. 3146.
[4] D. C. Ruspini, K. Kolarov, and O. Khatib, "The haptic display of complex graphical environments," in *SIGGRAPH '97: Proceedings of the 24th annual conference on Computer graphics and interactive techniques*. New York, NY, USA: ACM Press/Addison-Wesley Publishing Co., 1997, pp. 345–352.
[5] M. Ortega, S. Redon, and S. Coquillart, "A six degree-of-freedom god-object method for haptic display of rigid bodies with surface properties," *IEEE Trans. on Vis. and Comp. Graph.*, vol. 13, no. 3, pp. 458–469, 2007.
[6] M. Bro-Nielsen and S. Cotin, "Real-time volumetric deformable models for surgery simulation using finite elements and condensation," *Computer Graphics Forum*, vol. 15, no. 3, pp. 57–66, 1996.
[7] S. Cotin, H. Delingette, and N. Ayache, "Real-time elastic deformations of soft tissues for surgery simulation," *IEEE Trans. on Vis. and Comp. Graph.*, vol. 5, no. 1, pp. 62–73, January-March 1999.
[8] D. L. James and D. K. Pai, "A unified treatment of elastostatic contact simulation for real time haptics," *Haptics-e, the Electronic Journal of Haptics Research*, vol. 2, no. 1, 2005.
[9] J. Barbič and D. L. James, "Real-time subspace integration for st. venant-kirchhoff deformable models," in *SIGGRAPH '05: ACM SIGGRAPH 2005 Papers*, 2005, pp. 982–990.
[10] ——, "Six-dof haptic rendering of contact between geometrically complex reduced deformable models," *IEEE Trans. Haptics*, vol. 1, no. 1, pp. 39–52, 2008.
[11] D. Harmon, E. Vouga, B. Smith, R. Tamstorf, and E. Grinspun, "Asynchronous contact mechanics," *ACM Transactions on Graphics*, vol. 28, no. 3, p. 1, 2009.
[12] F. Barbagli, D. Prattichizzo, and K. Salisbury, "A Multirate Approach to Haptic Interaction with Deformable Objects Single and Multipoint Contacts," *The International Journal of Robotics Research*, vol. 24, no. 9, pp. 703–715, 2005.
[13] O. R. Astley and V. Hayward, "Multirate haptic simulation achieved by coupling finite element meshes through norton equivalents," in *Proc.of Int.Conf. on Robotics and Automation*, 1998, pp. 989–994.
[14] M. C. Cavusoglu and F. Tendick, "Multirate simulation for high fidelity haptic interaction with deformable objects in virtual environments," in *Proceedings of ICRA IEEE Int.Conf. on Robotics and Automation Symposia*, vol. 3, 2000, pp. 2458–2465.
[15] G. Debunne, M. Desbrun, M.-P. Cani, and A. H. Barr, "Dynamic real-time deformations using space & time adaptive sampling," in *Proc. of the 28th Conf. on Comp. graphics and Int. Tech.* New York, NY, USA: ACM, 2001, pp. 31–36.
[16] M. A. Otaduy and M. Gross, "Transparent rendering of tool contact with compliant environments," in *WHC '07: Proceedings of the Second Joint EuroHaptics Conference and Symposium on Haptic Interfaces for Virtual Environment and Teleoperator Systems*. Washington, DC, USA: IEEE Computer Society, 2007, pp. 225–230.
[17] G. Saupin, C. Duriez, and S. Cotin, "Contact model for haptic medical simulations," in *ISBMS '08: Proceedings of the 4th international symposium on Biomedical Simulation*. Berlin, Heidelberg: Springer-Verlag, 2008, pp. 157–165.
[18] C. Garre and M. A. Otaduy, "Haptic rendering of complex deformations through handle-space force linearization," in *Proc. of World Haptics Conference*, 2009, pp. 422–427.
[19] ——, "Toward haptic rendering of full-hand touch," in *Proc. of CEIG (Spanish Computer Graphics Conference)*, 2009.
[20] P. Jacobs, M. J. Fu, and M. C. Cavusoglu, "High Fidelity Haptic Rendering of Frictional Contact with Deformable Objects in Virtual Environments using Multi-rate Simulation," *The International Journal of Robotics Research*, 2010.
[21] G. Böttcher, D. Allerkamp, and F.-E. Wolter, "Multi-rate coupling of physical simulations for haptic interaction with deformable objects," *The Visual Computer*, vol. 26, no. 6-8, pp. 903–914, 2010.